

Pamukkale Üniversitesi Mühendislik Bilimleri Dergisi

Pamukkale University Journal of Engineering Sciences



Tumumate smy erotoy je ar nar or Engineering serences

The effects of rotor design on the performance of ipm-bldc motors in axial fan applications

Eksenel fan uygulamalarında rotor tasarımının ipm-bldc motorların performansı üzerindeki etkileri

Berk Demirsoy^{1*}, Buğra Er¹, Ahmet Fenercioğlu²

¹Kormas Electric Motor Inc., Tosb Organized Industrial Zone, Kocaeli, Türkiye. berkdemirsoy@kormas.com, bugraer@kormas.com

²Department of Mechatronics Engineering, Bursa Technical University, Bursa, Türkiye. ahmet.fenercioglu@btu.edu.tr

Received/Geliş Tarihi: 18.04.2025 Accepted/Kabul Tarihi: 06.10.2025 Revision/Düzeltme Tarihi: 02.09.2025 doi: 10.65206/pajes.42724 Research Article/Araştırma Makalesi

Abstract

This study investigates the influence of rotor design on the performance of interior permanent magnet brushless DC (IPM-BLDC) motors used in axial fan applications, which span from industrial cooling systems to automotive technologies. Two alternative rotor topologies with a 12/8 slot-pole configuration were analyzed using finite element analysis (FEA). The evaluation focused on key performance metrics, including torque ripple, cogging torque, and efficiency. The optimized flux-barrier rotor demonstrated a 55.36% reduction in cogging torque, a 1.23% improvement in efficiency, and a 2.23% decrease in torque ripple relative to the baseline design. Based on these results, the superior rotor geometry was prototyped, and the numerical findings were experimentally validated through performance testing. The outcomes confirm that rotor flux-barrier optimization enhances the overall efficiency and operational stability of IPM-BLDC motors in axial fan applications.

Keywords: IPM, Axial fan, Flux barrier, BLDC motor

1 Introduction C

Axial flow fans are used in a wide range of applications, from air conditioning systems to the cooling of compact electronic equipment. These fans play a critical role in HVAC (Heating, Ventilation, and Air Conditioning) systems by providing airflow [1]. Axial fans operate by pushing air in the axial direction using the swirling tangential motion created by the rotating fan blades [2]. The geometry of an axial flow fan is shown in Figure 1.

Axial fans are widely used in various vehicles for heating, cooling, ventilation, and engine cooling purposes [3]. Along with technological developments in the automotive industry, the required characteristics of motors used in axial fans have also advanced [4]. The basic characteristics expected from these motors include long life, low noise levels, high efficiency, compact design, low cost, and lightweight construction [5]. As an alternative to induction motors used in industrial applications, brushless DC (BLDC) motors have emerged as an ideal solution for fan systems due to their high efficiency, low energy consumption, compact size, and speed control features. BLDC motors deliver superior performance in terms of efficiency due to their high power-to-weight ratio, minimal

endüstriy el sistemlerinden çalışma, oğutma teknolojilerine kadar (e.i. bi) kullanım alanına sahip eksenel fan uygulamalarında ku lan an içten mıknatıslı firçasız doğru akım (IPM-BLDC) motorların performansı üzerindeki rotor tasarımının etkisini 8 oluk–kutup konfigürasyonuna sahip iki alternatif incelemektedin 1 rotor topolviisi sonlu elemanlar analizi (FEA) yöntemiyle değerlend rilmiştir. İnceleme; tork dalgalanması, vuruntu torku ve topolojisi sonlu elemanlar analizi (FEA) yöntemiyle verimlar şib temel performans metriklerine odaklanmıştır. Opunizasyonu yapılmış akı bariyerli rotor, referans tasarıma kıyasla vrunty torkunda %55,36 azalma, verimlilikte %1,23 artış ve tork dalşal nmasında %2,23 düşüş sağlamıştır. Bu sonuçlara dayanarak ♥üstün performans gösteren rotor geometrisi prototiplenmiş ve sayısal bulgular performans testleriyle deneysel olarak doğrulanmıştır. Elde edilen sonuçlar, akı bariyeri optimizasyonunun IPM-BLDC motorlarının eksenel fan uygulamalarındaki genel verimliliğini ve çalışma kararlılığını artırdığını doğrulamaktadır.

Anahtar kelimeler: IPM, Eksenel fan, Akı bariyeri, BLDC motor

maintenance requirements, and precise speed-torque control. Additionally, low rotor inertia enables rapid acceleration and deceleration, making them advantageous for dynamic applications [6-7].



Figure 1. Geometry of an axial-flow fan.

Öz

^{*}Corresponding author/Yazışılan Yazar

BLDC motors are commonly used in power transmission, electric HVAC compressors, cooling fans, and pumps. The ease of speed control, high efficiency, and long life cycle expectations make them a frequently preferred option for fan applications [8-9]. Generally, these motors are classified as surface-permanent magnet (SPM) and interior-permanent magnet (IPM) designs [10]. Figure 2 shows images of SPM and IPM motor structures.

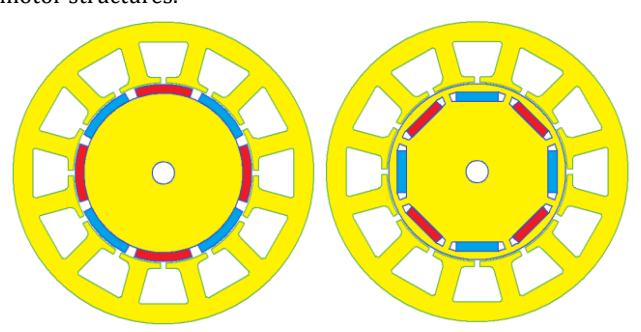


Figure 2. (a): SPM motor. (b): IPM motor.

Both motor types are known for their high torque density and efficiency. However, IPM motors also feature reluctance torque and offer advantages such as an extended speed range [11].

In IPM motors, flux barrier designs are crucial for improving torque ripple and cogging torque. Various techniques, such as adding additional holes or notches to the rotor surface, have been documented in the literature [12-13]. Furthermore, creating additional flux barriers can reduce leakage flux and thus increase the average torque. These modifications to the rotor can alter the back EMF waveform and reduce iron losses.

In general, the primary approach is to reduce reluctance along the d-axis and increase it along the q-axis, thereby achieving typical characteristics such as the d-axis inductance being greater than the q-axis inductance ($L_d > L_q$). However excessively increasing the flux barriers along the q-axis can lead to saturation in the flux path of the d-axis [14]. The flux paths along the d and q-axes are intricately interconnected and are directly influenced by the arrangement of the magnets. Therefore, the precise positioning of the flux barriers on the rotor is crucial [15].

The torque produced by IPM motors is fundamentally divided into two types: electromagnetic torque and reluctance torque. Electromagnetic torque arises from the interaction between the magnetic fields of the stator and rotor, while reluctance torque arises from the reluctance difference between the d-axis and q-axis [16].

The rotor of an IPM motor consists of permanent magnets made of either rare-earth or ferrite materials. Although ferrite magnets are more economical than NdFeB magnets, their lower remanent flux density (Br), energy density, and coercivity (–Hc) restrict their use to low-performance applications [17]. Since the present work requires high power density, sintered NdFeB magnets may be preferred; however, only sintered NdFeB was employed as the rare-earth magnet in this study [18].

In a similar study, the total bridge width was reduced by removing the two side bridges on the IPM motor rotor and leaving only the center bridge; this was shown to improve torque production by increasing the air gap flux density. This arrangement provided a 7.5% increase in torque and a 0.18% increase in efficiency in a comparative evaluation [19].

This study presents performance comparisons for axial fan applications based on modifying the flux barrier architecture in the rotor of a flat-type IPM-BLDC motor. In the first phase of the study, a reference motor was selected; the motor design was optimized using nominal operating points derived from the axial fan load, and preliminary FEA results were compared with the initial design. Subsequently, the final design obtained from the rotor geometry optimization was prototyped, and the measured performance curves were evaluated. The findings indicate that significant performance improvements were achieved in the Model 1 design for the axial fan motor, thus confirming the suitability of the proposed flux barrier arrangement for application.

2 Motor design for axial fans: Finite element analysis and comparative evaluation

A reference axial fan–motor model was utilized to determine the initial design parameters. Based on this model, the fan operates at approximately 225 W of electrical power at 2850 rpm, drawing 8.6 A from a 26 V supply, thereby defining the nominal operating point. Since the reference axial fan is known to draw 8.6 A at 0 Pa pressure, the fan blades were removed and the motor alone was subjected to a torque test. To replicate the fan load, the current was increased to 8.6 A, and the corresponding torque applied to the motor was measured as 0.64 N·m. From these performance measurements, the nominal operating point and the average fan load were derived. These results were then adopted as the initial constraints for the electromagnetic design of the IPM motor, providing guidance for the subsequent design process.

In IPM motors, selecting similar slot and pole numbers increases the winding factor, facilitating higher torque production. Additionally, slot-pole combinations that are close to each other result in lower cogging torque [20].

Although the motor used in this study has an IPM structure, sixstep BLDC commutation was preferred as the drive method. In IPM motors, the total torque consists of the electromagnetic torque component as well as the reluctance torque component. The torque relationship is given in Equation (1).

$$T = \frac{3}{2} p \left(\Phi_m i_q + (L_d - L_q) i_d i_q \right)$$
 (1)

p is the number of pole pairs, Φ_m is the magnetic flux, \mathbf{i}_d is the d-axis current, \mathbf{i}_q s the q-axis current [21].

In the six-step BLDC drive method, since the current vector is not controlled separately on the d–q axis, it is not possible to effectively optimize the reluctance torque component. In this case, the reluctance torque engages at a limited level and in an uncontrolled manner, while the main torque component is the electromagnetic torque, also known as the magnet torque. The new torque relationship for $i_d \approx 0$ is given in Equation (2).

$$T = \frac{3}{2} p \, \Phi_m i_q \tag{2}$$

Current vector-based methods such as field-oriented control (FOC) are required to utilize the reluctance torque contribution of the IPM motor most efficiently [22]. However, the reason for choosing BLDC drive due to simple control structure, low-cost driver requirement, and high applicability, which meet the targeted application requirements of the system.

The rotor design of the NdFeB-based IPM motor has been optimized using a multi-objective genetic algorithm (GA). During the optimization process, the parameters magnet width

 (w_m) , magnet thickness (d_m) , bridge thickness (w_{rib}) and flux-carrier thickness (dpc) were considered. Figure 3 shows the visual representation of the optimization parameters, and Table 1 provides the initial values of the IPM rotor.

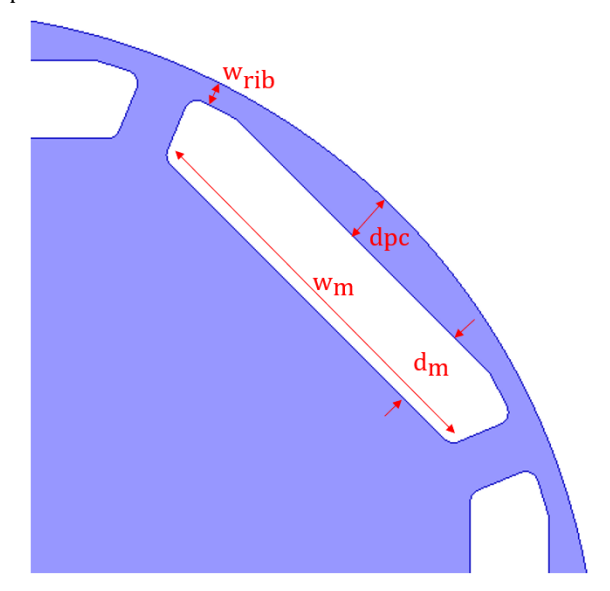


Figure 3. Initial geometry of the IPM rotor.

Table 1. Initial design parameters of the rotor.

Symbol	Parameters	Value
w_m	Magnet width [mm]	12
w_{rib}	Bridge thickness [mm]	1
dpc	Flux carrier thickness [mm]	2
d_m	Magnet thickness [mm]	3.2

The leakage factor (K_l) , is a critical parameter in IPM rotor design, representing the portion of the total magnetic flux generated by the permanent magnets that effectively passes through the air gap to contribute to torque production. In IPM motors, the leakage flux is typically higher than in SPM motors, since the magnets are embedded within the rotor. The presence of iron paths surrounding the magnets causes part of the flux to short-circuit without reaching the air gap. For designs targeting high torque density, the leakage factor should be as close to unity as possible. The leakage factor is defined by the expression given in Equation (3).

$$R_l = \frac{\phi_p}{\phi_m} \tag{3}$$

 Φ_p is the pole flux and Φ_m is the magnetic flux.

The leakage factor can be raised closer to 1 by reducing the bridge thickness or enlarging the magnet volume. However, in the optimization process, an excessive reduction in bridge thickness may compromise the mechanical integrity of the rotor [23]. Likewise, increasing the magnet volume may raise both the cost and weight of the motor. The variation of the leakage factor with respect to the optimization parameters is illustrated in Fig. 4, while the final dimensions of the IPM rotor are summarized in Table 2.

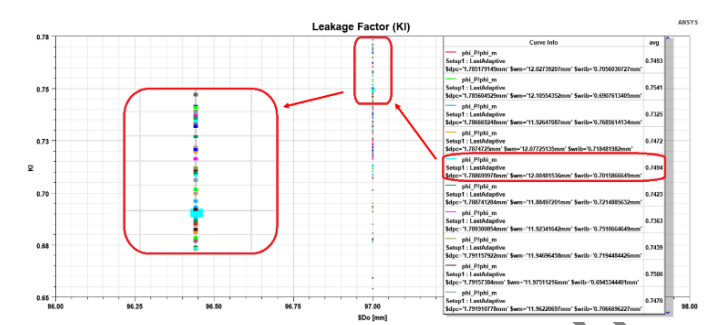


Figure 4. Optimization of IPM rotor leakage factor.

Table 2. Final design parameters of the rotor.

Symbol	Parameters	Value
w_m	Magnet width [mm]	12
w_{rib}	Bridge thickness [mm]	0.6
dpc	Flux carrier thickness [mm]	1.85
d_m	Magnet thickness [mm]	3

As a result of the optimization study, the design with the highest leakage factor and the most suitable dimensions for manufacturability was selected, yielding a leakage factor of 0.7494. The rotor was then operated at a speed approximately 20% above the nominal value and subjected to static strength analysis, which confirmed its mechanical integrity [24]. Furthermore, an additional locking groove was introduced into the magnet bearing to prevent magnet displacement caused by centrifugal and electromagnetic forces during operation. The static strength analysis results of the final rotor design are presented in Fig. 5.

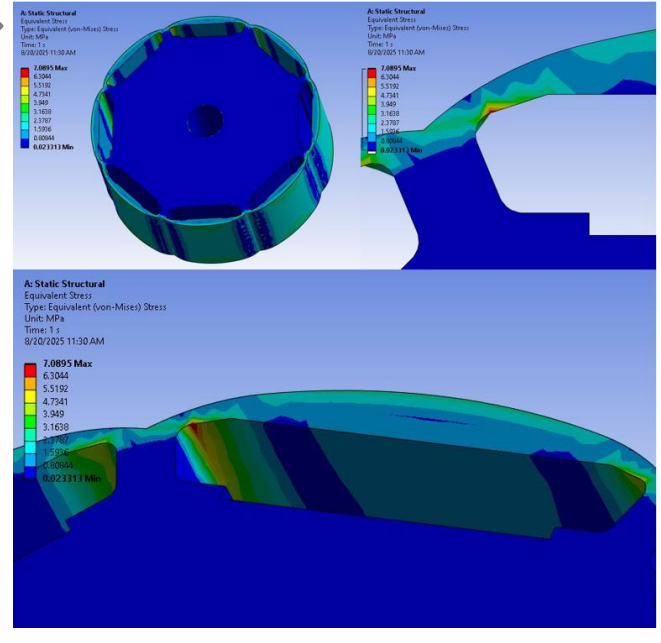


Figure 5. Final IPM rotor geometry static structural analysis.

The core material properties of the M470-50A electrical steel sheet were defined, the rotor was rotated at 3600 rpm, and the analysis outputs were examined. The results showed that the maximum stress was concentrated in the bridge regions. This stress, which reached a maximum level of 7.089 MPa, was confirmed by the analysis to pose no risk to the mechanical integrity of the rotor, as it remained within safe limits.

The final design Model 1 and initial design Model 2 2D finite element models of the IPM-BLDC motors are presented in Figure 6. Both machines have a 97 mm outer stator diameter, 20 mm stack (axial) length and a 12/8 slot-pole topology. The performance of the two different rotor types was compared through a comprehensive electromagnetic analysis.

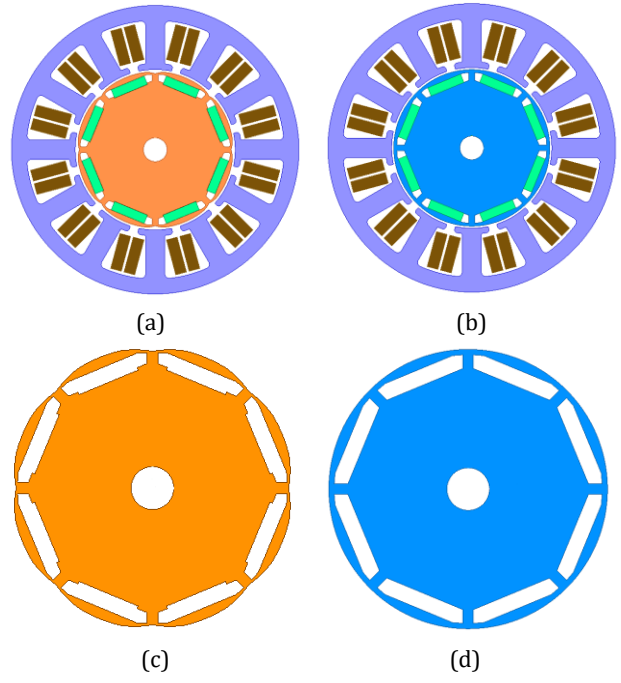


Figure 6. 2D models and rotor designs of Model 1 and Model 2 motors. (a): Model 1 2D motor model. (b): Model 2 2D motor model. (c): Model 1 2D rotor model. (d): Model 2 2D rotor model.

Although both designs have similar dimensions and magnet types, the fundamental difference lies in the additional flux barriers integrated into the outer surface of the rotor laminations in Model 1. Due to these design differences, Model 1 reached a nominal speed of 3025 rpm during the analysis phase, while Model 2 reached 2950 rpm. Table 3 shows the design parameters of these IPM-BLDC motors.

Table 3. Design parameters of ipm-bldc motors

Parameter	Model 1	Model 2
Stator Outer Diameter [mm]	97	97
Stack Length [mm]	20	20
Air Gap [mm]	0.7	0.7
Nominal Speed [rpm]	3025	2950
Phase Resistance [ohm] (at 60°C)	0.082	0.082
Magnet Type	NdFeB	NdFeB
Magnet Flux Density (B _r) [T]	1.21	1.21
Air Gap Flux Density (B_{av}) [T]	0.461	0.445

The designs were analyzed using Ansys Maxwell 2D electromagnetic simulation software within the scope of transient finite element analysis (FEA). Each motor model was run for a 150 ms simulation process, and the current/torque waveforms reached a steady state at approximately 40 ms. In similar studies, the average transition time to steady state has been reported as 70 ms [25].

According to FEA results:

- Model 1 rotor motor operated at 26V, with a phase current of 10.2A and reached a speed of 3025 rpm. It consumed 250.26W of electrical power and provided 202.7W of mechanical power.
- Model 2 rotor motor operated at the same voltage, with a phase current of 11.15A, reaching a speed of 2950 rpm. It consumed 249.88W of electrical power and provided 197.75W of mechanical power.

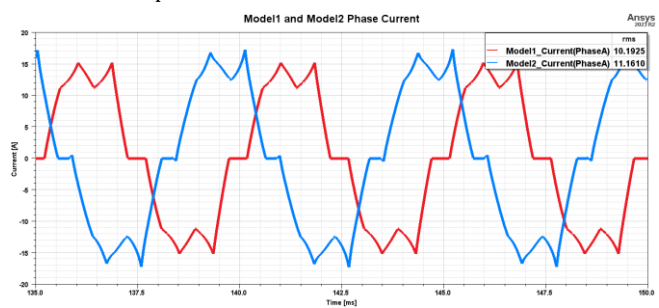
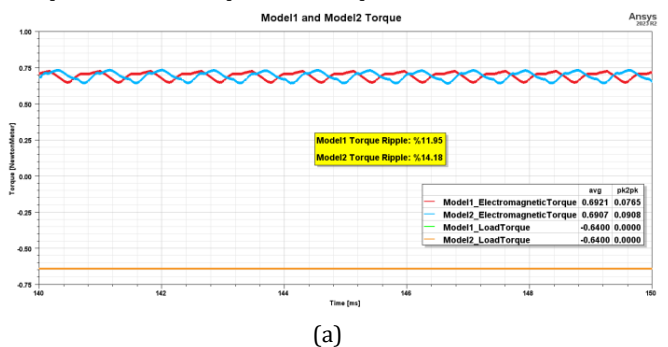


Figure 7. Phase current graphs for Model 1/Model 2 designs.

Under a constant load of 0.64 Nm, the electromagnetic torque value was determined to be 0.6921 Nm (red curve) for the Model 1 design and 0.6907 Nm (blue curve) for the Model 2 design. Analysis of torque ripple revealed that the torque ripple ratio was 11.95% for the Model 1 design and 14.18% for the Model 2 design. In the speed graph, it was observed that the nominal speed under load reached 3025 rpm for the Model 1 design (shown in red) and 2950 rpm for the Model 2 design (shown in green). Figure 8 shows the torque and speed characteristics of both motor designs under nominal load. These findings highlight the performance differences between the two designs and provide a comprehensive and reliable comparison of their operational capabilities.



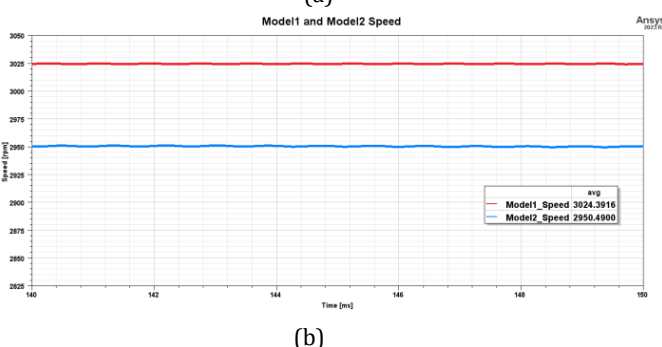


Figure 8. (a): Torque graph of Model 1 and Model 2 motors under nominal load. (b): Speed graph of Model 1 and Model 2 motors under nominal load.

A transient analysis was performed without energizing the stator windings to analyze the opposing EMF signals of the motors. The rotor was freely rotated around its axis using a drive motor at no-load speed. The EMF induced in the phases was observed on an oscilloscope.

The schematic diagram of the applied system is shown in Figure 9, while Figure 10 shows the simulation results of the phase-to-phase back EMF signals for the motors.

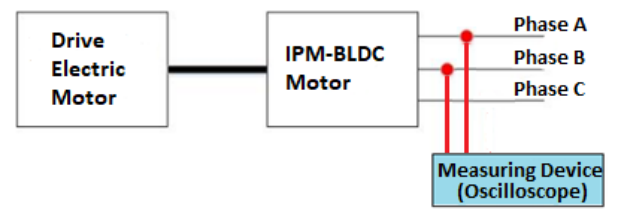


Figure 9. Schematic of back EMF signal measurement.

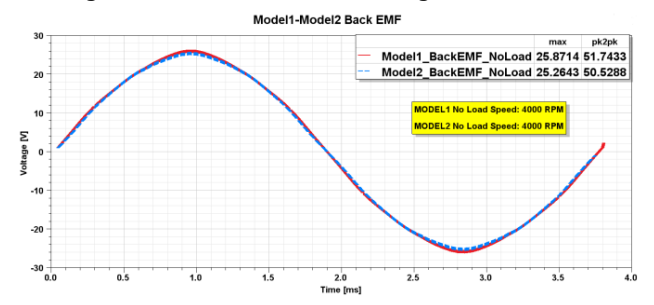


Figure 10. Back EMF waveforms of Model 1 and Model 2.

The sinusoidal nature of the back-EMF signal indicates that the motor will have lower torque ripple [26]. Based on the back-EMF waveforms, it was observed that the signal of Model 1 motor is closer to a sinusoidal shape. This indicates that Model 1 will have lower acoustic noise and vibration levels under load compared to Model 2. Additionally, when torque ripple percentages are considered, Model 1 exhibits approximately 2.23% less torque ripple than Model 2.

While cogging torque can be beneficial in some stepper motor applications, it is generally detrimental for permanent magnet (PM) motors [27]. Cogging torque is the source of harmonic magnetic forces in the stator and causes radial vibrations. This problem is particularly undesirable in medium and low-power PM motors because it causes vibrations and acoustic noise [28].

In the cogging torque analysis performed for two rotor geometries, $14.55~\text{mN}\cdot\text{m}$ was obtained for Model 1 and $32.61~\text{mN}\cdot\text{m}$ for Model 2. By adding additional flux barriers to the rotor geometry, the cogging torque was optimized and reduced by approximately 55.36%. The cogging torque waveforms and peak values for both designs are presented in Figure 11.

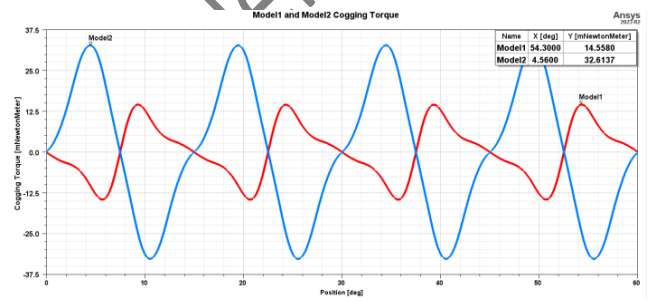


Figure 11. Simulation graph of cogging torque for Model 1 and Model 2.

To prevent saturation in the stator and rotor cores, the magnetic flux density must be maintained within a specific range [29]. The analysis results indicate that the maximum flux density reached 2.25 T in Model 1 and 2.16 T in Model 2. In both

models, the flux density in the stator teeth was approximately 1.61 T. Although localized core saturation was observed at the rotor edges, which may adversely affect efficiency, it also provides a flux-leakage inhibiting effect. The distributions of magnetic flux density (B) and current density (J) for both models are illustrated in Fig. 12.

	Name	х	Υ	Z	В	
	m1	25.825	11.591	-0.000	1.610e+0	0
	m2	28.822	19.506	-0.000	1.502e+0	0
	m3	16.221	19.982	0.000	1.979e+0	0
B [tes	sla] _				J	[A/m^2]
Max: 2	.258				L	lax: 5.450E+06
	2.300					6.0E+06
:	2.070					4.8E+06
	1.840				-	3.6E+06
	1.610					2.4E+06
	1.380				.	1.2E+06
	1.150			20		0.0E+00
	0.920			"" ²		-1.2E+06
	0.690					-2.4E+06
	0.460		1/1.00			-3.6E+06
	0.230					-4.8E+06
	0.000				-	-6.0E+06
Min: 0.	002				N	lin: -5.450E+06
	Name	x	γ (a) z	В	
•	m2	35.371	20.674	0.000	1.611	+00
	m3	16.172	20.233	-0.000	2.025	+00
	m4	26.236	11.272	0.000	1.701	+00
ВІ	[tesla]			_		
					[,	J [A/m^2]
Ma	x: 2.159				ļ.	
Ma					ļ.	
Ma	x: 2.159				ļ.	Max: 5.879E+06
Ma	x: 2.159 2.200				ļ.	Max: 5.879E+06 6.0E+06
Ma	2.200 1.980				ļ.	Max: 5.879E+06 6.0E+06 4.8E+06
Ma	2.200 1.980 1.760				ļ.	6.0E+06 4.8E+06 3.6E+06
Ma	2.200 1.980 1.760 1.540			m2	ļ.	Max: 5.879E+06 6.0E+06 4.8E+06 3.6E+06 2.4E+06
Ma	2.200 1.980 1.760 1.540 1.320			m2	ļ.	Max: 5.879E+06 6.0E+06 4.8E+06 3.6E+06 2.4E+06 1.2E+06
Ma	2.200 1.980 1.760 1.540 1.320 1.100			m2	ļ.	Max: 5.879E+06 6.0E+06 4.8E+06 3.6E+06 2.4E+06 1.2E+06 0.0E+00
Mai	2.200 1.980 1.760 1.540 1.320 1.100 0.880			"m2	ļ.	Max: 5.879E+06 6.0E+06 4.8E+06 3.6E+06 2.4E+06 1.2E+06 0.0E+00 -1.2E+06
Mai	2.200 1.980 1.760 1.540 1.320 1.100 0.880 0.660			,m2	ļ.	Max: 5.879E+06 6.0E+06 4.8E+06 3.6E+06 2.4E+06 1.2E+06 0.0E+00 -1.2E+06 -2.4E+06
	2.200 1.980 1.760 1.540 1.320 1.100 0.880 0.660 0.440			,m2		Max: 5.879E+06 6.0E+06 4.8E+06 3.6E+06 2.4E+06 1.2E+06 0.0E+00 -1.2E+06 -2.4E+06 -3.6E+06

Figure 12. (a): Magnetic flux density (B) and current density (J) simulation results for the Model 1 motor. (b): Magnetic flux density (B) and current density (J) simulation results for the Model 2 motor.

(b)

When examining the current densities of the two motors, the maximum current density for Model 1 is $5.45~\text{A/mm}^2$, while for Model 2 it is $5.87~\text{A/mm}^2$. A comparison of the copper losses specific to the designs, as can be understood from the current density values, shows that Model 1 has lower copper loss than Model 2. These results highlight the effect of the designs on energy efficiency and show that Model 1 has an advantage in terms of copper loss.

3 Final design and prototype production

The performance comparison of two different BLDC motors was performed using 2D transient analysis in Ansys Maxwell electromagnetic simulation software. The solutions are summarized in Table 4.

Table 4. Comparison of output characteristics for two different

Parameter	Model 1	Model 2
Input Voltage [V]	26	26
Torque [Nm]	0.64	0.64
Source Current [A]	9.63	9.6
Phase Current [A _{rms}]	10.2	11.15
Pin [W]	250.26	249.88
Pout [W]	202.7	197.75
Copper Loss [W]	25.75	30.77
Core Loss [W]	11.51	12.69
Efficiency [%]	81	79.77

According to the comparison of the analysis results, Model 1's rotor geometry was found to be 1.23% more efficient and was accepted as the final design for the axial fan motor. Figure 13 shows the stator laminations, rotor laminations, wound stator assembly, magnetized rotor assembly, and the final IPM-BLDC motor design.

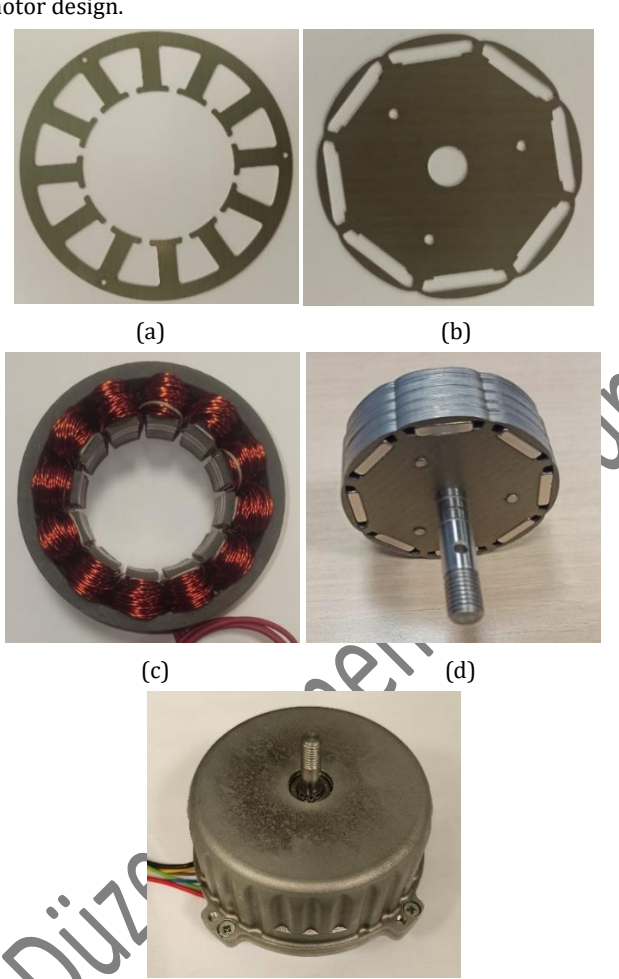


Figure 13. (a): Stator lamination. (b): Rotor lamination. (c): Wound stator core. (d): Magnetized rotor core. (e): Final IPM-BLDC motor design.

(e)

Following the completion of the IPM BLDC motor prototype, detailed tests were conducted to measure its performance. The purpose of these tests was to determine the motor's design and technical characteristics, evaluate its performance, and verify its suitability for specific application requirements. Prior to the performance tests, a system was set up to check whether the

back-EMF signal was sinusoidal. During this process, the rotor was rotated at no-load speed using the drive motor without energizing the stator windings. A servo motor was used to bring the test motor to its no-load speed of 4000 rpm, and the back-EMF signal induced in the windings was observed on an oscilloscope via probes connected to two phases. Figure 14 shows the back-EMF signal test systems, while Figure 15 shows the measured back-EMF signal.

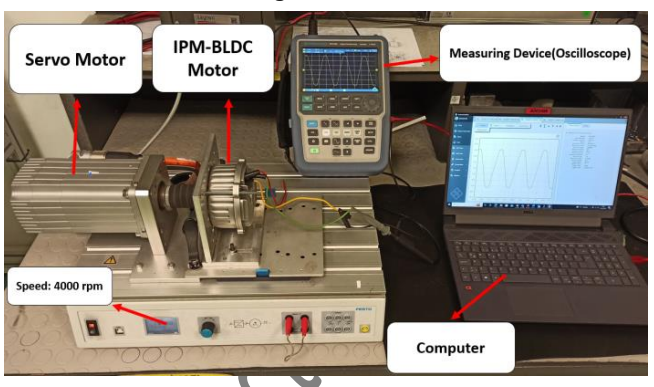


Figure 14. Back EMF signal test system.

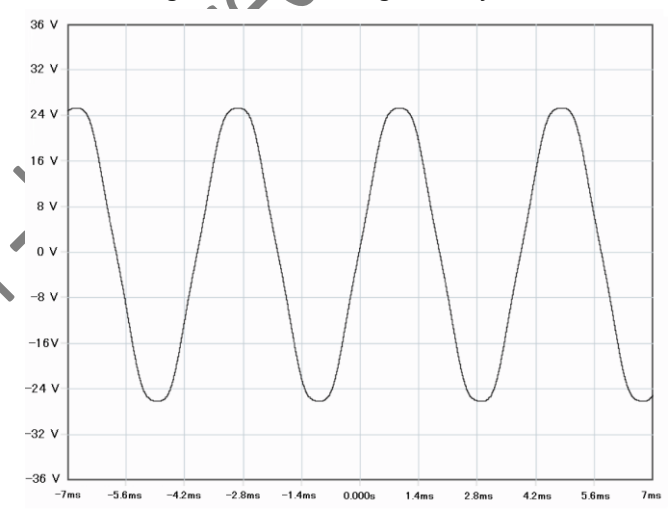


Figure 15. Back EMF signal of the IPM-BLDC motor.

The testing process was conducted on various operational scenarios to understand how the motor behaves under different conditions. These comprehensive tests measured critical parameters such as speed, torque, current, and efficiency to evaluate how well the design met its objectives. The testing phase is crucial for validating the motor before moving to mass production. The data obtained will be used to evaluate whether the motor's performance meets expectations and to make any necessary adjustments. A visual representation of the test setup is shown in Figure 16.

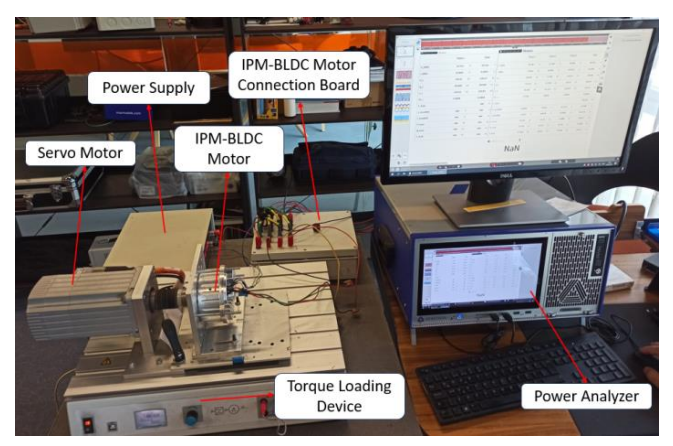


Figure 16. Test system for the IPM-BLDC motor.

During the tests, the system was powered through a regulated supply, and the motor driver was connected via an interface card. The IPM-BLDC motor was loaded using a servo motor under various load conditions, and its operating performance was evaluated with a Dewetron power analyzer. The performance characteristics of the tested IPM-BLDC motor are presented in Fig. 17.

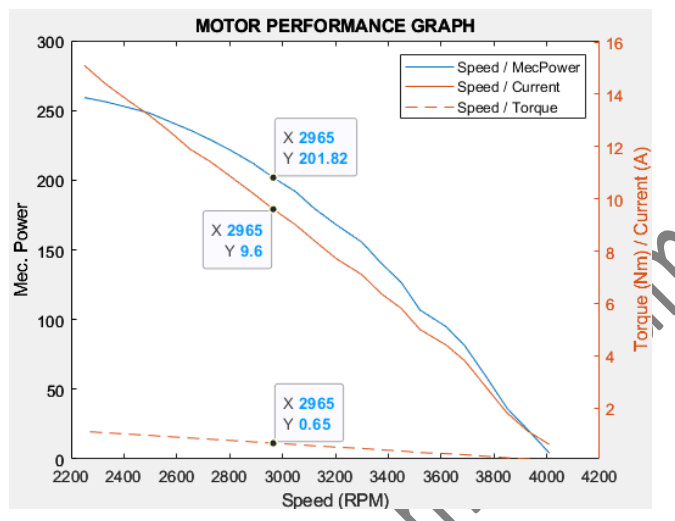


Figure 17. Performance curves of the IPM-BLDC motor.

From the torque/speed, torque/mechanical power, and current/speed performance curves shown in Figure 17, it can be observed that as the applied load increases, the current draw and output power also increase, while the speed decreases. The test data shows that the nominal operating values of the IPM-BLDC motor were obtained at a load of 0.65 Nm, a speed of 2965 rpm, a current of 9.6A, and an efficiency of 80.8%.

4 Conclusion

In this study, two IPM-BLDC motor rotor designs (Model 1 and Model 2) were compared for improving the performance of axial fans in commercial vehicle HVAC systems. Model 1 exhibited superior performance under load, characterized by lower torque ripple and cogging torque, as well as enhanced operational stability through a more linear speed profile. The maximum flux density in the Model 1 rotor reached 2.25 T locally; although local core saturation was observed, optimized flux barriers effectively reduced both iron and copper losses.

These design enhancements resulted in a 55.36% reduction in cogging torque, a 1.23% improvement in efficiency, and a

2.23% reduction in torque ripple for Model 1 compared to Model 2. Consequently, the Model 1 rotor geometry was identified as a more suitable and efficient configuration for axial fan applications.

Comprehensive analyses confirm the positive impact of the Model 1 design on motor performance, energy efficiency, and operational reliability. With advantages including higher efficiency, reduced torque ripple, and lower maintenance requirements, the Model 1 rotor stands out as a promising solution for high-performance axial fan applications in the automotive industry.

5 Author contribution statements

Author 1 designed the rotor, performed finite element analyses, interpreted the prototype motor test results, and contributed to the writing of the article.

Author 2 analyzed the performance parameters of the prototype motor and contributed to the writing of the article.

Author 3 supervised the rotor design and finite element analyses and revised the article for writing and grammar accuracy.

6 Ethics committee approval and conflict of interest statement

"There is no need to obtain permission from the ethics committee for the article prepared."

"There is no conflict of interest with any person / institution in the article prepared."

7 References

- [1] Abu-Ramadan E, Dybenko J, Savory E, Hunt AG, Martinuzzi RJ. "Stator and Support Arm Aerodynamic Performance for Automotive Engine Cooling Fans with Realistic Inlet Conditions". SAE Transactions, 116(6), 687–697, 2007.
- [2] Goetzler W, Guernsey M, Chung G. "Pump and fan technology characterization and R&D assessment". Navigant Consulting, Burlington, USA, No. DOE/EE-1268, 2015.
- [3] Williams EE, Didandeh H, Cahill KM. "Design of an innovative high-efficiency fan for engine cooling". Vehicle Thermal Management Systems Conference and Exhibition (VTMS10), Gaydon, United Kingdom, 15-19 May 2011.
- [4] Cory W. Fans and Ventilation: A Practical Guide. 1st ed. Oxford, UK, Elsevier Science, 2010.
- [5] Ebm-Papst. "Automotive BL-DC Fans for Commercial Vehicles. Product Catalog. 2019-10". https://www.ebmpapst.com/de/en/support/downloads/brochures-and-catalogs.html (28.04.2025).
- [6] Liu CS, Hwang JC. "Development of brushless DC motor with low cogging torque for ceiling fan". IEEE 2009 International Conference on Power Electronics and Drive Systems (PEDS), Tokyo, Japan, 2-5 November 2009.
- [7] Reddy KA, Champa V, Nalawade PS. "Development of speed control for high voltage BLDC ceiling fan using regulator". 2021 IEEE Mysore Sub Section International Conference (MysuruCon), Mysuru, India, 21-23 October 2021.
- [8] Lee GC, Jung TU. "Design comparisons of BLDC motors for electric water pump". 2012 IEEE Vehicle Power and Propulsion Conference, Seoul, South Korea, 9-12 October 2012.
- [9] Lelkes A, Bufe M. "BLDC motor for fan application with automatically optimized commutation angle". 2004 IEEE

- 35th Annual Power Electronics Specialists Conference (IEEE Cat. No. 04CH37551), Toledo, Spain, 20-25 June 2004.
- [10] Zhao W, Zhao F, Lipo TA, Kwon BI. "Optimal design of a novel V-type interior permanent magnet motor with assisted barriers for the improvement of torque characteristics". *IEEE Transactions on Magnetics*, 50(11), 1-4, 2014.
- [11] Parasiliti F, Villani M, Lucidi S, Rinaldi F. "Finite-element-based multiobjective design optimization procedure of interior permanent magnet synchronous motors for wide constant-power region operation". *IEEE Transactions on Industrial Electronics*, 59(6), 2503-2514, 2011.
- [12] Kioumarsi A, Moallem M, Fahimi B. "Mitigation of torque ripple in interior permanent magnet motors by optimal shape design". *IEEE Transactions on Magnetics*, 42(11), 3706-3711, 2006.
- [13] Huang S, Liu J, Gao J, Xiao L. "Optimal design of the rotor structure for interior permanent magnet synchronous motor". 2011 International Conference on Power Engineering, Energy and Electrical Drives, Munich, Germany, 11-13 May 2011.
- [14] Zhu X, Wu W, Yang S, Xiang Z, Quan L. "Comparative design and analysis of new type of flux-intensifying interior permanent magnet motors with different q-axis rotor flux barriers". *IEEE Transactions on Energy Conversion*, 33(4), 2260-2269, 2018.
- [15] Ocak C, Dalcalı A. "Gömülü mıknatıslı senkron motorların geometrik tabanlı akı bariyeri optimizasyonu". *Journal of Awareness*, 3(5), 225-234, 2019.
- [16] Putri AK, Hombitzer M, Franck D, Hameyer K. "Comparison of the characteristics of cost-oriented designed high-speed low-power interior PMSM". *IEEE Transactions on Industry Applications*, 53(6), 5262-5271, 2017.
- [17] Isfanuti AS, Baba M, Tutelea L, Moldovan A, Boldea I. "Surface NdFeB versus Ferrite IPM motor drive for low power (100W to 2000W) applications: FEM embedded optimal design with full step torque response validation in sensorless vector control". 2013 IEEE 39th Annual Conference of the IEEE Industrial Electronics Society (IECON), Vienna, Austria, 10-13 November 2013.
- [18] Gundogdu T, Komurgoz G. "The impact of the selection of permanent magnets on the design of permanent magnet machines—a case study: permanent magnet synchronous

- machine design with high efficiency". *Przegląd Elektrotechniczny R89*, 103-108, 2013.
- [19] Shao B, Cai W, Yang C. "Electromagnetic-thermal-mechanical performance of novel interior permanent magnet motor". Case Studies in Thermal Engineering, 63, 105259, 2024.
- [20] Jafarishiadeh S, Ardebili M, Marashi AN. "Investigation of pole and slot numbers in axial-flux PM BLDC motors with single-layer windings for electric vehicles". 2016 24th Iranian Conference on Electrical Engineering (ICEE), Tehran, Iran, 17-19 May 2016.
- [21] Cho S, Jeong G, suk Lim J, Oh YJ, Ham SH, Lee J. "Characteristics analysis of novel outer rotor fan-type pmsm for increasing power density". *Journal of Magnetics*, 23(2), 247-252, 2018.
- [22] Garmut M, Steentjes S, Petrun M. 'Optimization of an IPMSM for Constant-Angle Square-Wave Control of a BLDC Drive". *Mathematics*, *12*(10), 1418, 2024.
- [23] Mi C, Filippa M, Liu W, Ma R. "Analytical method for predicting the air-gap flux of interior-type permanent-magnet machines". *IEEE Transactions on Magnetics*, 40(1), 50-58, 2004.
- [24] Yang F, Li N, Du G, Huang M, Kang Z. "Electromagnetic Optimization of a High-Speed Interior Permanent Magnet Motor Considering Rotor Stress". *Applied Sciences* (2076-3417), 14(14), 2024.
- 3417), 14(14), 2024.
 [25] Kim HK, Hur J. "Dynamic characteristic analysis of irreversible demagnetization in SPM-and IPM-type BLDC motors". *IEEE Transactions on Industry Applications*, 53(2), 982-990, 2016.
- [26] Lu H, Zhang L, Qu W. "A new torque control method for torque ripple minimization of BLDC motors with un-ideal back EMF". *IEEE Transactions on Power Electronics*, 23(2), 950-958, 2008.
- [27] Hanselman DC. Brushless Permanent Magnet Motor Design. The Writers' Collective, 2nd ed. 2003.
- [28] Sumega M, Rafajdus P, Stulrajter M. "Current harmonics controller for reduction of acoustic noise, vibrations and torque ripple caused by cogging torque in PM motors under FOC operation". *Energies*, 13(10), 2534, 2020.
- [29] Çelik H, Çetin NS. "For different industrial applications: Outer rotor and low speed induction machine design". Journal of the Faculty of Engineering and Architecture of Gazi University, 38(4), 2009-2023, 2023.